Journal of Inorganic Biochemistry 197 (2019) 110674

Contents lists available at ScienceDirect

Journal of Inorganic Biochemistry

journal homepage: www.elsevier.com/locate/jinorgbio

Reactivity of bio-inspired Cu(II) (N2/Py2) complexes with peroxide at room temperature

Nirupama Singh[a], Niharika Krishna Botcha[a], Thomas M. Jones[a], Mehmed Z. Ertem[b], Jens Niklas[c], Erik R. Farquhar[d], Oleg G. Poluektov[c], Anusree Mukherjee[a,*]

[a] Department of Chemistry, University of Alabama in Huntsville, 301 Sparkman Drive, Huntsville, AL 35899, United States of America
[b] Chemistry Division, Brookhaven National Laboratory, Upton, New York 11973-5000, United States of America
[c] Chemical Sciences and Engineering Division, Argonne National Laboratory, 9700 S. Cass Avenue, Lemont, IL 60439, United States of America
[d] Case Western Reserve University, Center for Synchrotron Biosciences, National Synchrotron Light Source II, Brookhaven National Laboratory, Upton, New York 11973-5000, United States of America

ARTICLE INFO

Keywords:
Cu-complexes reactivity with peroxide
Hydrocarbon oxidation

ABSTRACT

Developing coordination complexes of earth abundant metals that can perform substrate oxidations under benign conditions is an ongoing challenge. Herein, the reactivity of two mononuclear Cu-complexes toward the oxidant H_2O_2 is reported. Both complexes displayed ligand oxidation upon reaction with the oxidant. Analysis of spectroscopic data established that the respective product complexes contained mononuclear Cu(II) centers. Moreover, treatment of these Cu-complexes with oxidant in the presence of substrate resulted in the interception of ligand oxidation with preferential oxidation of the substrate. Computational studies identified plausible mechanistic pathways, suggesting a copper-oxyl intermediate as the likely reactive intermediate responsible for substrate and ligand oxidation. To our knowledge, this is the first Cu-mediated system that showed ligand oxidation, oxo-transfer capability, and external hydrocarbon oxidation under stoichiometric conditions.

1. Introduction

The functionalization of hydrocarbons in an environmentally benign manner is one of the greatest challenges of chemistry in the twenty-first century. Oxidative transformations are useful for hydrocarbon functionalization and are heavily involved in the conversion of petroleum feedstocks to building blocks for the synthesis of many useful chemicals and pharmaceutical compounds. Metabolic processes incorporating C—H bond oxidation can serve as inspiration for developing eco-friendly pathways for obtaining synthetic chemicals. In recent decades, there has been enormous progress in the development and incorporation of bio-inspired strategies to achieve regio- and stereoselective C—H bond oxidations [1].

In the literature, reactivity studies of Cu-complexes with hydrogen peroxide (H_2O_2) have primarily been performed in the interest of understanding the mechanism of the enzymes dopamine beta-monooxygenase and peptidylglycine alpha-hydroxylating monooxygenase [2]. These biomimetic studies have provided important insights that allowed key copper-oxygen adducts to be trapped and characterized [3]. Cu-complexes supported by the bispicen family of ligands with amine and pyridine functionalities can also serve as suitable functional models for the histidine-rich coordination environment of the copper active sites of lytic polysaccharide monooxygenase and particulate methane monooxygenase [4]. While the reactivity of mononuclear copper complexes toward dioxygen activation has been extensively investigated, reports of the reactivity of mononuclear copper complexes toward hydrogen peroxide remain limited [4–5]. This biomimicry provides valuable insight into the nature of copper-oxygen intermediate species and the factors that influence their formation and reactivity [3]. Previous studies have concluded that the reactivity of mononuclear Cu-complexes with H_2O_2 is mostly governed by the coordination geometry around the metal center [6]. Specifically, mononuclear complexes that generated a Cu(II)-hydroperoxo (Cu-OOH) intermediate with square pyramidal geometry exhibited substrate oxidation, while those with trigonal bipyramidal geometry displayed no reactivity [7]. Additionally, another study found that a Cu-OOH species with square pyramidal geometry showed oxidation of a ligand arm [8]. In all cases, the Cu-OOH species was implied as a reactive intermediate but the involvement of other intermediates could not be ruled out [8–9]. Mononuclear copper complexes have shown great promise for C—H bond activation using O_2 as the oxidant [4,10]. However, reports of mononuclear Cu- complexes that oxidize C—H bonds using hydrogen

* Corresponding author.
E-mail address: anusree.mukherjee@uah.edu (A. Mukherjee).

https://doi.org/10.1016/j.jinorgbio.2019.03.014
Received 16 October 2018; Received in revised form 5 March 2019; Accepted 18 March 2019
Available online 21 March 2019
0162-0134/

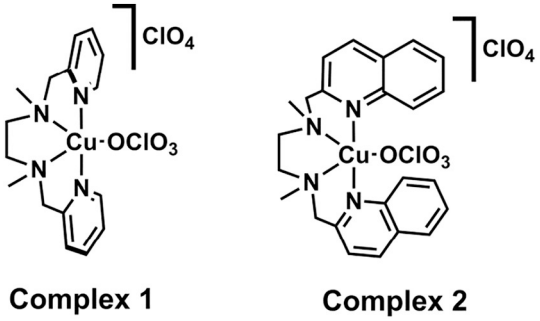

Fig. 1. Copper complexes studied in the present work.

peroxide as an oxidant remain limited.

In the present work, we have explored the reactivity of two mononuclear complexes in square pyramidal geometry with H_2O_2 as the oxidant. BPMEN (*N,N′*-dimethyl-*N,N′*-bis-(pyridine-2-ylmethyl)-1,2-diaminoethane), a ligand from the bispicen family, has already been reported to support mononuclear Cu-complexes in a square pyramidal geometry [11]. Here, through a combined experimental and computational approach, we examine the reactivity of two Cu-complexes, [Cu(BPMEN)$(ClO_4)_2$] (**1**) and its quinoline derivative (BQDMEN: *N,N′*-dimethyl-*N,N′*-bis-(quinoline-2-ylmethyl)-1,2-diaminoethane) [Cu(BQDMEN)$(ClO_4)_2$] (**2**) (Fig. 1), with H_2O_2, and show that the oxidant generated from both complexes performs ligand oxidation that can be intercepted by the addition of triphenylphosphine and external hydrocarbons.

2. Experimental

2.1. Materials and methods

All reagents and solvents were purchased from Sigma-Aldrich and Fisher Scientific and directly used for synthesis without further purification unless otherwise mentioned. Copper complexes and ligands were synthesized following reported procedures [11]. 9,10-Dihydroanthracene (DHA) was purchased from Sigma-Aldrich and recrystallized from ethanol prior to use [12]. All electronic absorption spectra were measured using an Agilent Cary 8454 UV–Vis (Ultraviolet–Visible) Spectrophotometer equipped with a Unisoku low-temperature cryostat. Samples for optical spectroscopy were prepared in quartz cells with an optical path length of 1 cm. The electrospray ionization mass spectrometry (ESI-MS) experiments were performed with a Thermo Scientific LTQ Orbitrap XL Hybrid Fourier Transform Mass Spectrometer (FT-MS) in positive ionization mode. Graphical representation and data analysis were performed in Origin. Nuclear magnetic resonance (NMR) spectroscopy samples were prepared by redissolving the demetallated product solution in deuterated methanol (CD_3OD). All NMR experiments were carried out using a Varian 500 MHz spectrometer. Heteronuclear multiple bond correlation (HMBC) experiments were realized using the standard crisis2 heteronuclear multiple bond correlation (gc2hmbc) pulse sequence with a ^{13}C spectral width of 0–225 ppm, 256 t_1 increments, and 64 scans per t_1 increment. Band-selective HMBC experiments were realized using the band-selective gradient heteronuclear multiple bond correlation (bsgHMBC) pulse sequence with a ^{13}C spectral width of 153.1–202 ppm, 512 t_1 increments, and 32 scans per t_1 increment at a sampling density of 75%. Data processing was done using MestReNova (version 12.0.1).

Electron paramagnetic resonance (EPR) samples were prepared by removing the solvent from the product solution mixture and then redissolving the sample in an acetonitrile/dichloromethane (MeCN/DCM) 1:3 solvent mixture. All EPR spectroscopy experiments were carried out with a Bruker ELEXSYS II E500 EPR spectrometer (Bruker Biospin, Rheinstetten, Germany), equipped with a TE_{102} rectangular EPR resonator (Bruker ER 4102ST). A helium gas-flow cryostat (ICE Oxford, UK) and a temperature controller (ITC503; Oxford Instruments, UK) were used for measurements at cryogenic temperatures (T = 50 K). Data processing was done using Xepr (Bruker BioSpin) and Matlab 7.11.2 (The MathWorks, Inc., Natick) software environments. Simulations were performed using the EasySpin software package (version 5.1.8) [13].

X-ray absorption spectroscopy (XAS) spectra were obtained at the Stanford Synchrotron Radiation Lightsource (SLAC National Accelerator Laboratory, Menlo Park, CA) on beamlines 2-2 (**1**, **2**, and **2-Product**) and 9-3 (**1-Product**). SPEAR3 operated at 3.0 GeV and 500 mA in top-off mode. On beamline 2-2, a water-cooled Si(111) double-crystal monochromator was used for energy selection, detuned by 30–40% to reject higher harmonics. On beamline 9-3, a cryogenically-cooled Si(220) double-crystal monochromator was used for energy selection, with a Rh-coated harmonic rejection mirror before the monochromator rejecting higher harmonics (13 keV cutoff configuration) and a Rh-coated toroidal focusing mirror after the monochromator used for tuning beam focus. During data collection, samples were maintained at 20 K on beamline 2-2 with a He Displex cryostat and 10 K on beamline 9-3 with an Oxford liquid helium cryostat. A copper metal foil was collected simultaneously using a photodiode for internal energy calibration, with the first inflection point of the reference foil set to 8979.0 eV. XAS spectra were collected in fluorescence using 13 element (beamline 2-2) and monolithic 100 pixel (beamline 9-3) solid state germanium detectors (Canberra). On beamline 9-3, use of a Z-1 filter (6 μ Ni) and Soller slits was required to maintain detector linearity. Spectra were monitored for evidence of radiation damage during data collection, as indicated by progressive red-shifts in the absorption edge energy, and new spots on the sample exposed as necessary. XAS samples were prepared for **1**, **2**, **1-product** and **2-product** by freezing the starting materials and the final product solutions, respectively.

All XAS data were processed using Athena, while Artemis was used for extended X-ray absorption fine structure (EXAFS) analysis [14]. Theoretical phase and amplitude parameters were calculated for representative models of **1** and **2** using the FEFF6L program integrated into Artemis and the output inspected to identify significant paths. For a given shell, the coordination number n was fixed, while r and σ^2 were allowed to float. The amplitude reduction factor S_0^2 was fixed at 0.9, while the edge shift parameter ΔE_0 was allowed to float at a single common value for all shells. The fit was evaluated in k^3-weighted R-space, and fit quality was judged by the reported R-factor and reduced χ^2. Significant fits are tabulated in Tables S1–S4.

2.2. Reaction with H_2O_2

The reactions of **1** and **2** with H_2O_2 were performed in a UV–Vis cell under anaerobic conditions. Solutions of **1** and **2** were prepared in anhydrous acetonitrile (2 mM) and kept at room temperature. To this solution, triethylamine (NEt_3, 10 equivalents) and H_2O_2 (10 equivalents) were added using a gas tight syringe.

2.3. Demetallation studies

Demetallation studies were carried out as previously reported [15]. The reaction mixture was allowed to stir for 24 h at room temperature and was followed by the addition of ammonium hydroxide (2 mL, 28.0–30.0%). The resulting solution was passed through a mini-alumina column. The alumina column was washed with methanol (10 mL) followed by dichloromethane (20 mL). The combined filtrate was further washed with water (3 × 10 mL). The organic layer was collected and dried over sodium sulfate, and the solvent was removed in vacuo. Mass recovery was ca. 2 mg (ca. 60%, $[BPMEN + O\text{-}2H]^+$). Mass spectrometry was used to identify the product. The ^1H NMR spectrum of the demetallated solution indicated that while the degree of ligand

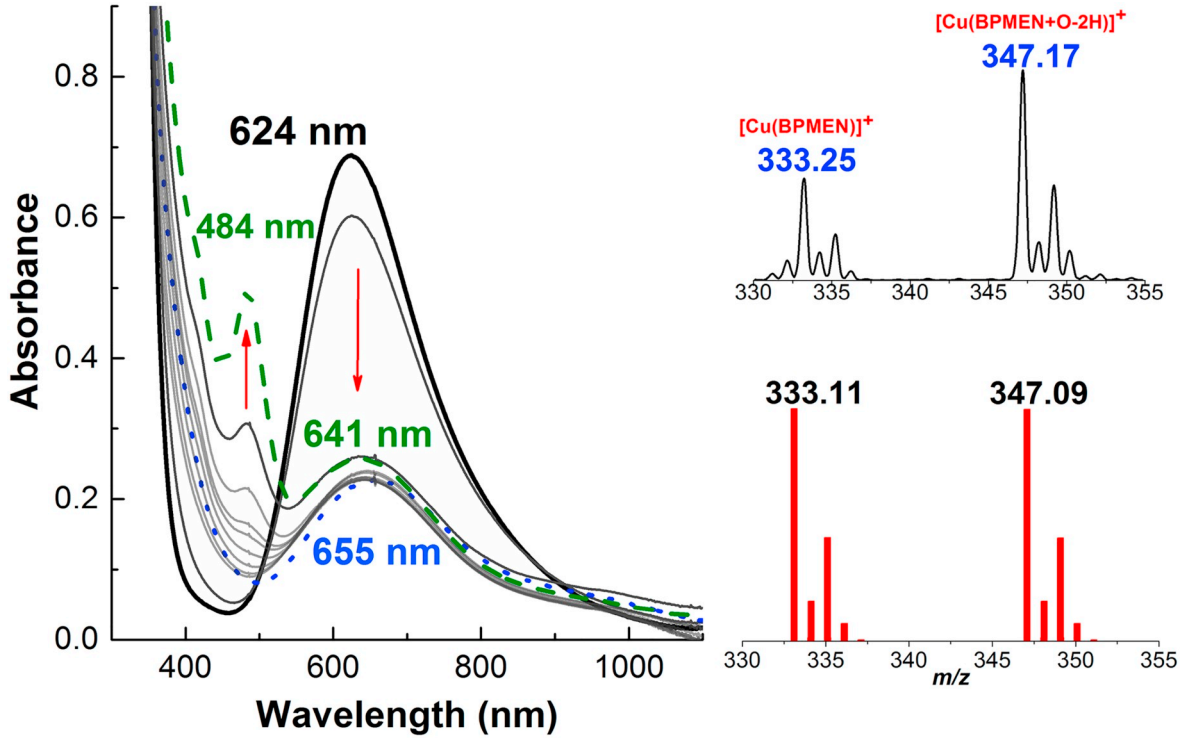

Fig. 2. Left panel: UV–visible spectral changes of complex **1** (black) upon addition of H_2O_2/NEt_3. The initial solution (2 mM, black solid line) immediately generates an intermediate solution (blue dash-dotted line) and slowly converts to a final solution (green dashed line) in acetonitrile at room temperature. Grey lines represent spectral changes over the time. Right Panel: ESI-MS spectrum of the final product solution of **1** (black, top) and its simulation (red, bottom).

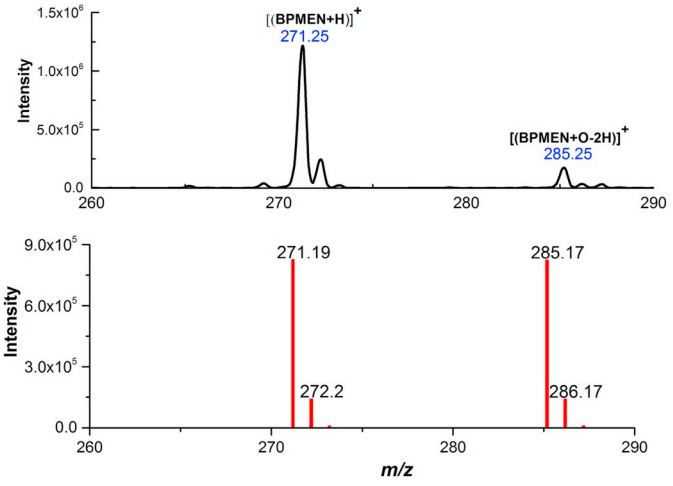

Fig. 3. ESI-MS spectra of demetallated solution from complex **1** (final green chromophore). (In red: software simulation of expected mass peaks).

oxidation is not high, oxidized product clearly has been formed. Diffusion-ordered spectroscopy (DOSY) indicated that the mixture was likely more complicated than originally anticipated. This was corroborated via HMBC experiments. The presence of two ^{13}C resonances at 169.4 ppm and 169.9 ppm in Fig. S1 were further resolved through a band-selective HMBC experiment (Fig. S1 inset). The data showed two distinct carbonyl signals that fall within the typical chemical shift range for amides [16]. The ^{13}C resonance 169.9 ppm was assigned to the amide product resulting from oxidation of the benzylic position, and the resonance at 169.4 ppm was assigned to the oxidation of the ligand's methylene backbone (one of the NC$\underline{H}_2$) [17]. The data suggest that the ligand is oxidized at two different positions, both of which correspond to the peak at m/z = 285, providing spectroscopic evidence that the mixture contains both oxidation products. Because of the similarity of the functional groups, the different products were not distinguished through other spectroscopic measurements.

A similar procedure was performed to demetallate complex **2** for which mass recovery was ca. 3 mg (ca. 27%, $[BQDMEN + O\text{-}2H]^+$). Product was similarly identified by ESI-MS spectroscopy. As the yield of ligand oxidation is lower with **2**, NMR analysis focused on complex **1** only.

2.4. Gas chromatography analysis of external substrates oxidation

Oxidation of external substrates was performed with complexes **1** and **2**. All solutions were kept under anaerobic conditions, and all experiments were performed, at minimum, in triplicate.

2.5. General procedure for substrate oxidation

In a sample solution of Cu-complexes, 40 equivalents of substrate were added, followed by the addition of H_2O_2 and NEt_3 solutions in acetonitrile (each 10 equivalents with respect to Cu-complex). Reaction progress was monitored with UV–Vis absorption spectroscopy, and products were identified after removal of the Cu-complex using a mini-alumina column. Quantification of the oxidized products was carried out with gas chromatography (GC) equipped with a flame ionization detector (FID) using naphthalene as an internal standard.

2.6. Computational methods

All geometries were fully optimized at the M06-L level of density functional theory [18] using the Stuttgart [8s7p6d2f|6s5p3d2f] ECP10MWB contracted pseudopotential basis set on Cu [19] and the 6-31G(d) basis set [20] on all other atoms. The grid = ultrafine option (in Gaussian 09 [21]) was chosen for integral evaluation, and an automatically generated density-fitting basis set was used within the resolution-of-the-identity approximation for the evaluation of Coulomb

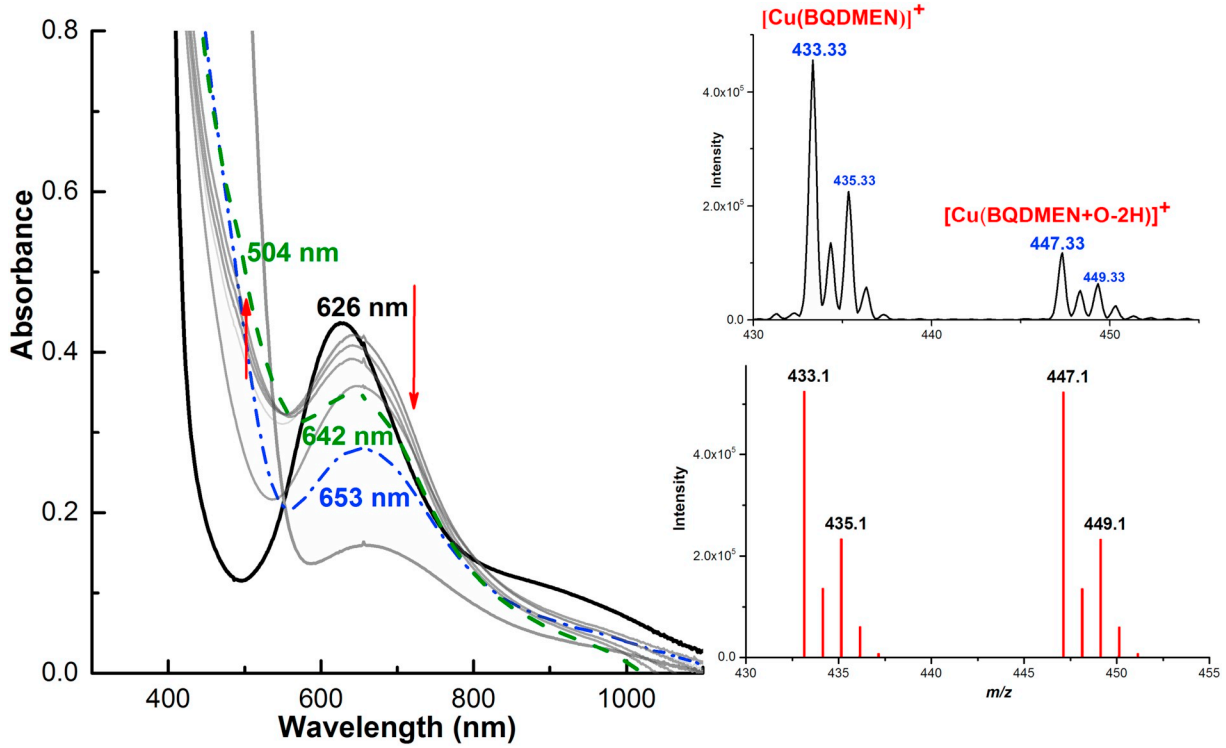

Fig. 4. Left panel: UV–vis absorption spectral changes of complex **2** (black, 2 mM) upon addition of NEt_3 and H_2O_2. The initially formed intermediate solution (blue dash-dotted line) slowly converted to final solution (green dashed line) in acetonitrile at room temperature. Grey lines represent spectral changes over the time. Right Panel: ESI-MS spectrum of the final product solution (upper panel) and simulated mass spectrum showing expected isotope pattern (lower panel).

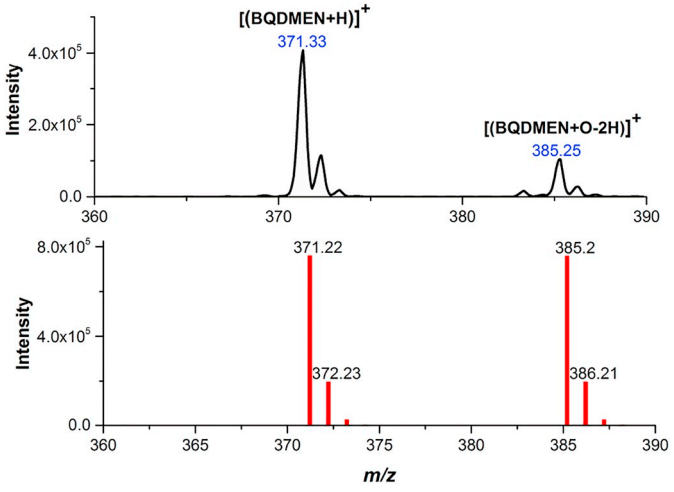

Fig. 5. ESI-MS spectra of demetallated solution from complex **2** (final green chromophore). (In red: software simulation of expected mass peaks).

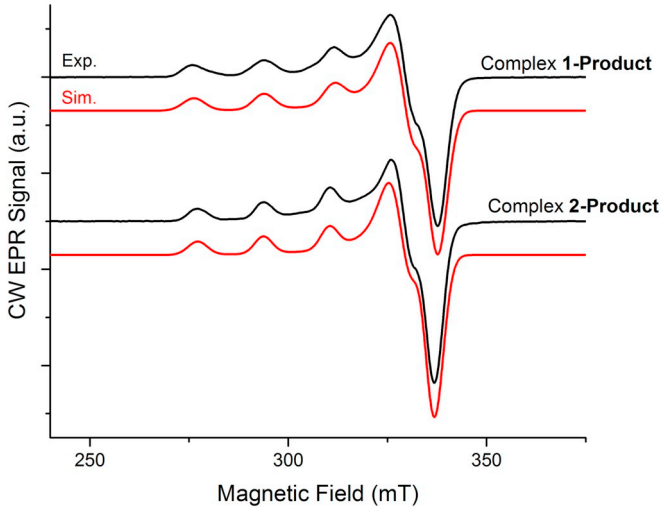

Fig. 6. CW X-band EPR spectra (at $T = 50$ K) of final product solutions from reactions of complexes **1** and **2** with H_2O_2/NEt_3 at room temperature in a 1:3 mixture of MeCN/DCM (see methods for details). Black – experimental spectra; red – simulated spectra. Simulation parameters are $g_{\parallel} = 2.238$, $g_{\perp} = 2.055$ and $A_{\parallel} = 181 \times 10^{-4}\,cm^{-1}$ for **1-Product** solution and $g_{\parallel} = 2.242$, $g_{\perp} = 2.054$ and $A_{\parallel} = 170 \times 10^{-4}\,cm^{-1}$ for **2-Product** solution. Cu hyperfine coupling constants are given for the ^{63}Cu isotope. The perpendicular value $A_{\perp}$ is not given, since the hyperfine structure is not clearly resolved. The simulations were performed assuming axial g-tensor and Cu A-tensors. In addition, it was assumed for the simulation that the principal g-tensor axes are collinear with the Cu A-tensor principal axes.

integrals. The nature of all stationary points was verified by analytic computation of vibrational frequencies, which were also used for the computation of zero-point vibrational energies, molecular partition functions, and for determining the reactants and products associated with each transition-state structure (by following the normal modes associated with imaginary frequencies).

Partition functions were used in the computation of 298 K thermal contributions to free energy employing the usual ideal-gas, rigid-rotator, harmonic oscillator approximation [22]. Solvation effects associated with acetonitrile as solvent were accounted for by using the SMD continuum solvation model [23]. A 1 M standard state was used for all species in solution thus, for all molecules, the free energy in solution is computed as the 1 atm gas-phase free energy, plus an adjustment for the 1 atm to 1 M standard-state concentration change of RT ln (24.5), or 1.9 kcal/mol, plus the 1 M to 1 M transfer (solvation) free energy computed from the SMD model. Free energy contributions were added to single-point M06-L electronic energies computed with the SDD basis

set on Cu and the 6-311 + G(2df,p) basis set on all other atoms to arrive at final, composite free energies.

Time-dependent density functional theory (TDDFT) calculations were performed to predict the UV/visible electronic excitations of relevant structures. The B3LYP density functional [24], Stuttgart [8s7p6d2f|6s5p3d2f] ECP10MWB contracted pseudopotential basis set on Cu [19] and the 6-311 + G(d,p) basis set [20] on all other atoms were used for the TDDFT calculations. Non-equilibrium solvation effects were included via the linear response approximations [25] in combination with the SMD aqueous continuum solvation model [23].

Standard reduction potentials were calculated for various possible redox couples to assess the energetic accessibility of different intermediates at various oxidation states. For a redox reaction of the form

$$O_{(soln)} + n\ e^-_{(g)} \rightarrow R_{(soln)} \quad (1)$$

where O and R denote the oxidized and reduced states of the redox couple, respectively, and n is the number of electrons involved in redox reaction, the reduction potential $E_{O|R}^{o}$ relative to SCE was computed as.

$$E^{o}_{O|R} = -\frac{\Delta G^{o}_{O|R}}{nF} - \Delta E^{o}_{ref} \quad (2)$$

where $\Delta G_{O|R}^{o}$ is the free energy change associated with Eq. (1) (using Boltzmann statistics for the electron) and ΔE_{ref}^{o} is taken as −4.422 V, which is required for the conversion of calculated $E_{O|R}^{o}$ relative to the vacuum level to $E_{O|R}^{o}$ versus the saturated calomel electrode (SCE) in acetonitrile [26].

3. Results and discussion

The syntheses of **1** and **2** and their characterization by different spectroscopic techniques have been reported [11]. Complexes **1** and **2** exhibit broad d-d transition bands at approximately 624 and 626 nm with a low-energy tail. Addition of H_2O_2 (10 equiv.) to a blue solution of **1** in acetonitrile (MeCN) in the presence of triethylamine (NEt_3,10 equiv.) at room temperature resulted in a rapid color change to green. This color change was accompanied by the decay of the 624 nm peak and generation of a new peak at 655 nm that subsequently disappeared to form a new product species with an absorption feature at 484 nm and a shoulder at 641 nm (Fig. 2). When the final product solution of complex **1** was analyzed by ESI-MS, a new peak at m/z = 347.17 was observed, along with the parent ion peak at m/z = 333.25. Both peaks exhibit similar isotopic distribution patterns (Fig. 2). The peak with m/z = 333.25 is consistent with a $[(BPMEN)Cu]^+$ formulation, suggesting that the addition of 14 mass units for m/z = 347.17 can be interpreted as addition of an oxygen atom to $[(BPMEN)Cu]^+$ with concomitant loss of two hydrogen atoms, resulting in the formation of [(BPMEN)Cu + O-2H]$^+$.

In order to determine whether the oxygen atom was inserted in the ligand, the product solution was demetallated with aqueous NH_4OH and extracted with dichloromethane. ESI-MS analysis of the extracted organic layer showed two peaks, one of which is readily assigned to protonated BPMEN ligand (m/z = 271), while the second at m/z = 285.25 corresponds to an oxygenated ligand $[BPMEN + O\text{-}2H]^+$ (Fig. 3), with yield of 60%.

Treatment of complex **2** in MeCN with H_2O_2/NEt_3 (10 equiv.) elicited similar changes. Specifically, the bluish-green solution of the starting material associated with the peak at 626 nm decreased in intensity and generated a final solution with dark green color with a peak at 642 nm along with a shoulder at ~504 nm (Fig. 4). Mass spectrometric analysis of the final solution showed two prominent peaks at m/z

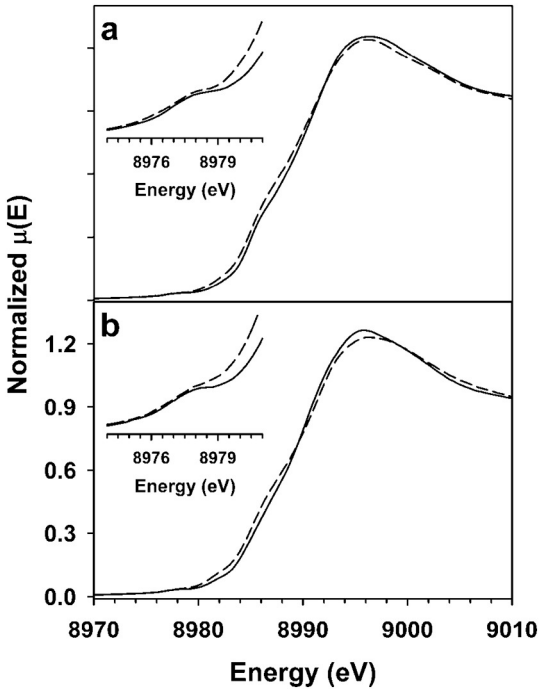

Fig. 7. Normalized XANES spectra of (a) **1** (——) and **1-Product** (- - -), (b) **2** (——) and **2-Product** (- - -). The insets show expansions of the pre-edge region.

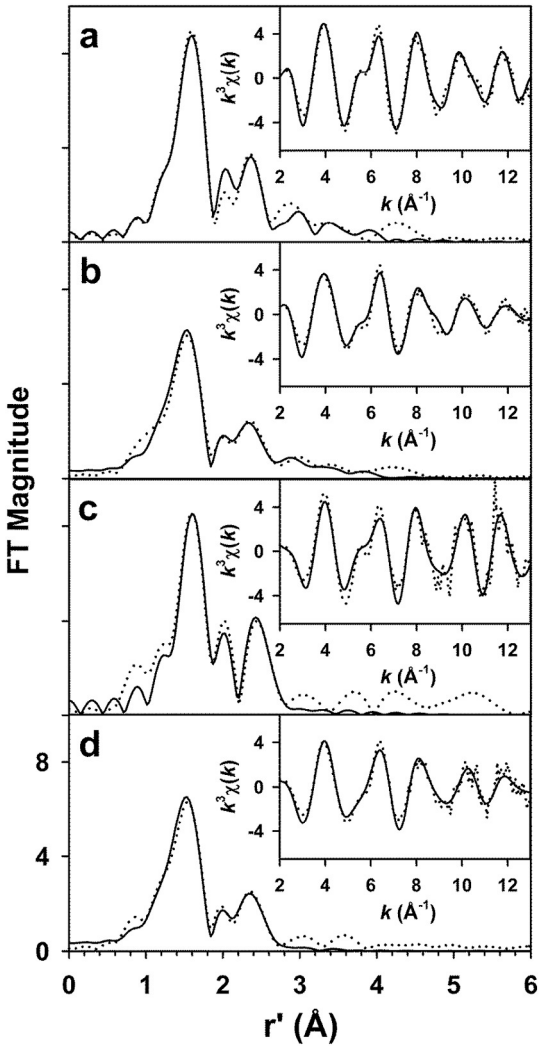

Fig. 8. Representative best fits (bolded entries in Tables S1–S4) to k^3-weighted EXAFS data of **1** (a), **1-Product** solution (b), **2** (c), and **2-Product** solution (d). Experimental data is shown as a dotted line while the best fit is shown as a solid line.

433.3 ([(BQDMEN)Cu]$^+$) and 447.3 ([(BQDMEN)Cu + O-2H]$^+$). The ligand oxidation product was isolated in 27% yield by demetallation and confirmed by mass spectrometry that showed a peak at m/z = 385 (Fig. 5).

In summary, these observations suggest that the reaction of complexes **1** and **2** with H_2O_2 at room temperature resulted in the oxidation of the ligand framework (Fig. S1). This is an important finding, as there are very few reports of ligand oxidation with mononuclear copper(II) complexes and H_2O_2/NEt_3 [3,8,27]. In order to corroborate the source of the oxygen atom inserted in the ligand, the reactions were performed in the presence of $H_2{}^{18}O_2$. Use of this isotopically labeled oxidant elicited a shift of the peak at m/z = 347 to m/z = 349, consistent with the matching simulation (Fig. S2). This result establishes that H_2O_2 is the source of the oxygen inserted in the ligand.

In order to establish the nature of the metallic species present in the product solution, we undertook additional spectroscopic studies of the final product solutions generated from **1** and **2**. Continuous wave (CW) X-band (9–10 GHz) EPR of frozen product solutions of **1** and **2** displayed axial EPR spectra, with $g_\parallel = 2.238$, $g_\perp = 2.055$ and $A_\parallel = 181 \times 10^{-4}\,cm^{-1}$ (^{63}Cu) for the **1-Product** solution and $g_\parallel = 2.242$, $g_\perp = 2.054$ and $A_\parallel = 170 \times 10^{-4}\,cm^{-1}$ (^{63}Cu) for the **2-Product** solution (Fig. 6). These values are typical for mononuclear Cu (II) complexes in square pyramidal geometry ($g_\parallel > 2.1 > g_\perp > 2.00$ and $A_\parallel = 158–201 \times 10^{-4}\,cm^{-1}$) suggesting that the major species in the final solution is also mononuclear in nature [28].

This was further corroborated by X-ray absorption spectroscopy. The X-ray absorption near edge structure (XANES) spectra (Fig. 7) of all four complexes show an extremely weak 1s-to-3d transition at 8977.8 eV and minimal structure along the rising edge, consistent with a Cu(II) center. Notably, spectra for both of the **1-Product** and **2-Product** solutions show somewhat weakened pre-edges and broadened edges relative to their respective precursors.

EXAFS analysis (Fig. 8, Tables S1–S4) establishes that all four complexes are best fit with a set of 5 nitrogen ligands at 1.98–2.02 Å. Complex **2** exhibits a slightly altered coordination environment, with 4 N at 2.03 Å and 1 N/O (presumably bound counter ion or solvent molecule) at 2.22 Å, in line with an apically distorted square pyramidal geometry. There is evidence that the other three complexes (**1**, **1-Product**, and **2-Product**) have a similarly distorted structure, however they could not be defensibly fit with two subshells of scatterers in the first coordination sphere.

The observation of ligand oxidation by **1** and **2** in the presence of H_2O_2 led us to investigate the reactivity of these complexes toward external substrates under similar conditions. We first examined oxo-transfer reactivity using triphenylphosphine (PPh_3). Addition of H_2O_2 to the solution of **1** in MeCN in the presence of excess PPh_3 (40 equiv.) resulted in the complete loss of the 624 nm peak assigned to **1**. No growth of the features at 483 nm and 641 nm associated with ligand oxidation was observed (Fig. 9). ESI-MS analysis of the faint-yellow product solution showed only a single peak at m/z = 333.25 corresponding to [(BPMEN)Cu]$^+$. No peak at m/z = 347.17 assignable to [(BPMEN)Cu + O-2H]$^+$ was observed (Fig. 9), which suggests that ligand oxidation was inhibited in the presence of phosphine. Analysis of the product solution using gas chromatography – mass spectrometry (GC–MS) showed the presence of triphenylphosphine oxide (Ph_3PO), indicating that **1** was able to oxidize PPh_3 in the presence of H_2O_2

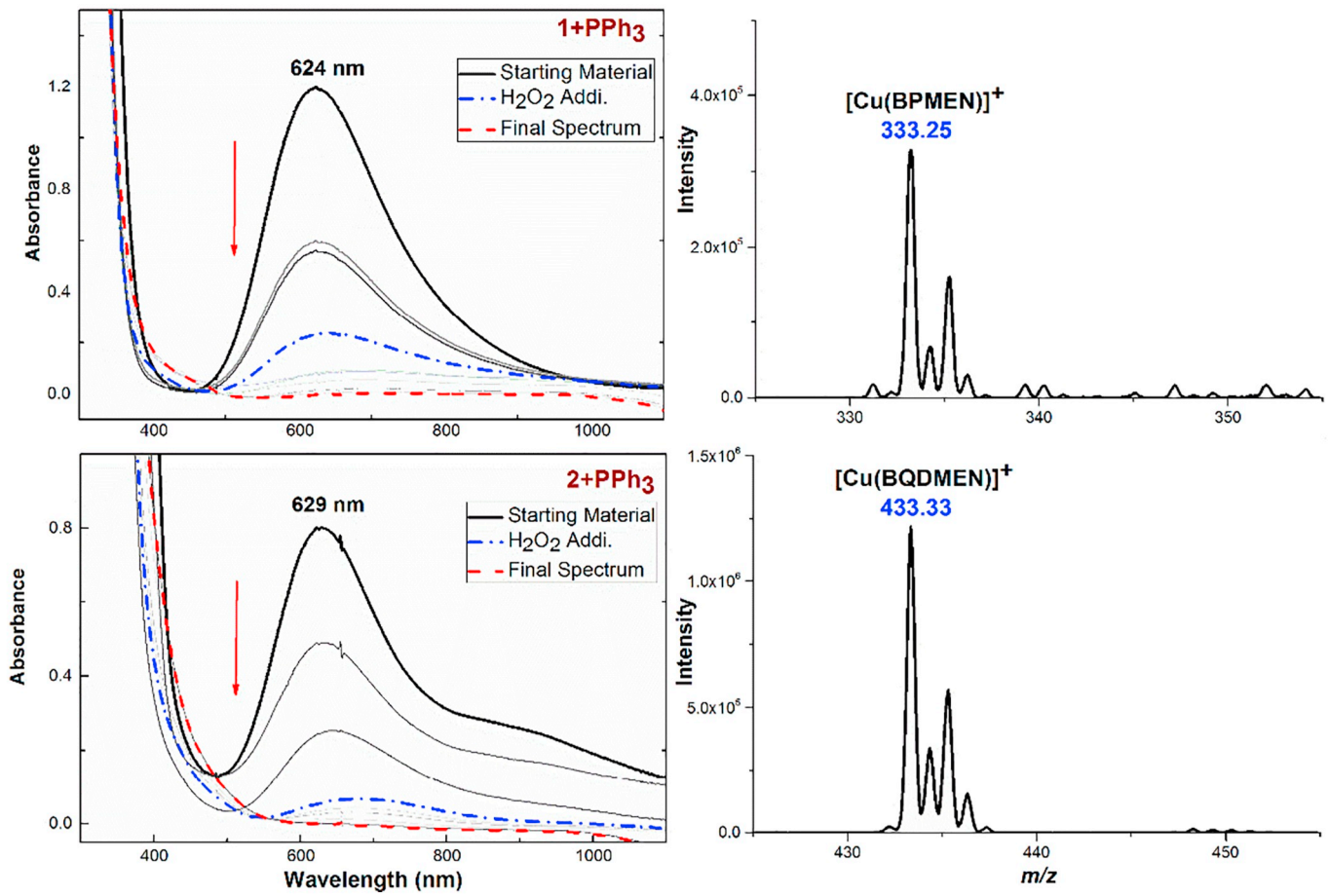

Fig. 9. UV–vis absorption spectral changes of complex **1** (2 mM, upper panel) and complex **2** (2 mM, lower panel) with H_2O_2/NEt_3 in the presence of excess PPh_3 (40 equivalents) in acetonitrile at room temperature in a cuvette with a 1-cm path length. On right side, ESI-MS spectra of the final product solution (Upper panel: complex **1** + PPh_3 + H_2O_2 / NEt_3, Lower panel: complex **2** + PPh_3 + H_2O_2 / NEt_3).

Table 1
Product analysis with different substrates.

Substrate	1 Product (%yield)	2 Product (%yield)
Triphenylphosphine (PPh_3)	O = PPh_3 (23%)	O = PPh_3 (35%)
9,10-Dihydro-anthracene (DHA)	Anthraquinone (8%) Anthracene (8%)	Anthraquinone (3%) Anthracene (4%)
1,4-Cyclo-hexadiene (CHD)	Benzene (68%)	Benzene (67%)

(Table 1). Complex **2**, when allowed to react with H_2O_2 in the presence of PPh_3, exhibited similar reactivity (Fig. 9 and Table 1).

With this intriguing result in hand, we then evaluated whether **1** and **2** were capable of reacting with hydrocarbons as exogenous substrates. It is noteworthy that no mononuclear Cu-complexes reported thus far showed external hydrocarbon oxidation with H_2O_2 except under catalytic conditions [29]. We explored the reactivity of 9,10-dihydroanthracene (DHA, 77 kcal/mol) and 1,4-cyclohexadiene (CHD, 78 kcal/mol) under our conditions. Both substrates have weak C—H bonds, but access toward the weakest C—H bond is more sterically demanding for DHA compared to CHD [30]. Oxidation of **1** and **2** in the presence of excess hydrocarbons (40 equiv.) resulted in absorption spectra (Figs. 10 and 11) that were significantly different than those observed without substrate (Figs. 2 and 4).

Analyses of the product solutions using GC–MS established that both substrates were oxidized. In the case of DHA, both anthraquinone and anthracene were identified as products, while benzene was obtained as the major product of CHD oxidation (Table 1). The product yields were calculated with respect to complexes **1** and **2**. When the hydrocarbon oxidation reactions were attempted with copper(II) perchlorate or with tetrakis(acetonitrile)copper(I) tetrafluoroborate, addition of H_2O_2 resulted in precipitation, suggesting that the reactivity displayed by **1** and **2** arises because of their unique ligand environment. Furthermore, no measurable amount of hydrocarbon oxidation was observed using only oxidant in the absence of **1** and **2** (with PPh_3 we found 2% of product Ph_3PO under this condition). Collectively, our reactivity studies show that **1** and **2** are able to oxidize the ligand, perform oxo-transfer to a phosphine substrate, and oxidize external hydrocarbons using H_2O_2 as the oxidant.

Density functional theory (DFT) calculations at the M06-L level of theory [18] with the SMD continuum solvation model [23] for acetonitrile were performed to investigate the possible pathways for ligand and external substrate oxidation by complex **1**. A proposed mechanism for ligand oxidation with H_2O_2 starting from **[1-MeCN]** $^{2+}$ is presented in Scheme S1. Here we will focus on the critical step of hydrogen atom abstraction by proposed Cu^{II}-OOH (**[1-OOH]** $^{+}$) and $Cu^{II}O^{\cdot -}$ (**[1-O]** $^{+}$) species.

The optimized geometries of **[1-MeCN]** $^{2+}$ and **[1-OOH]** $^{+}$ at the M06-L level of theory and computed UV–Vis spectra at the TD-B3LYP level of theory [24] confirm the square pyramidal geometry around the copper center and the nature of the associated electronic bands (Figs. S3–S4). The intermediate **[1-OOH]** $^{+}$ features three distinct sites for C-H activation, specifically, benzylic CH_2, bridging CH_2 and amine CH_3 groups. The oxidation kinetics of the ligand at these distinct sites was probed by examining the free energy of activation ($\Delta G^{\ddagger}$) associated with hydrogen atom abstraction by either (i) the distal oxygen atom (with respect to the Cu center) or (ii) the proximal oxygen atom of **[1-OOH]** $^{+}$ with concomitant O—O bond cleavage. The latter pathway (ii) was found to be consistently more favorable, and optimized transition state (TS) structures along with the associated $\Delta G^{\ddagger}$ values for hydrogen atom abstraction from distinct sites of the ligand by **[1-OOH]** $^{+}$ are listed in Fig. S5 along other TS structures. We have provided further details in the supporting information on the description and energetics of the optimized transition states, and we will focus only on the relevant ones for the discussion here. Among the several sites considered, H-abstraction from CH_3 groups on the amine nitrogens features the lowest activation free energy, with $\Delta G^{\ddagger}$ of 22.7 kcal/mol (TS-1a, Fig. 12), whereas $\Delta G^{\ddagger}$ is computed to be 37.1 kcal/mol for the benzylic CH_2 groups (TS-1b, Fig. 12). Furthermore, we found H-abstraction from

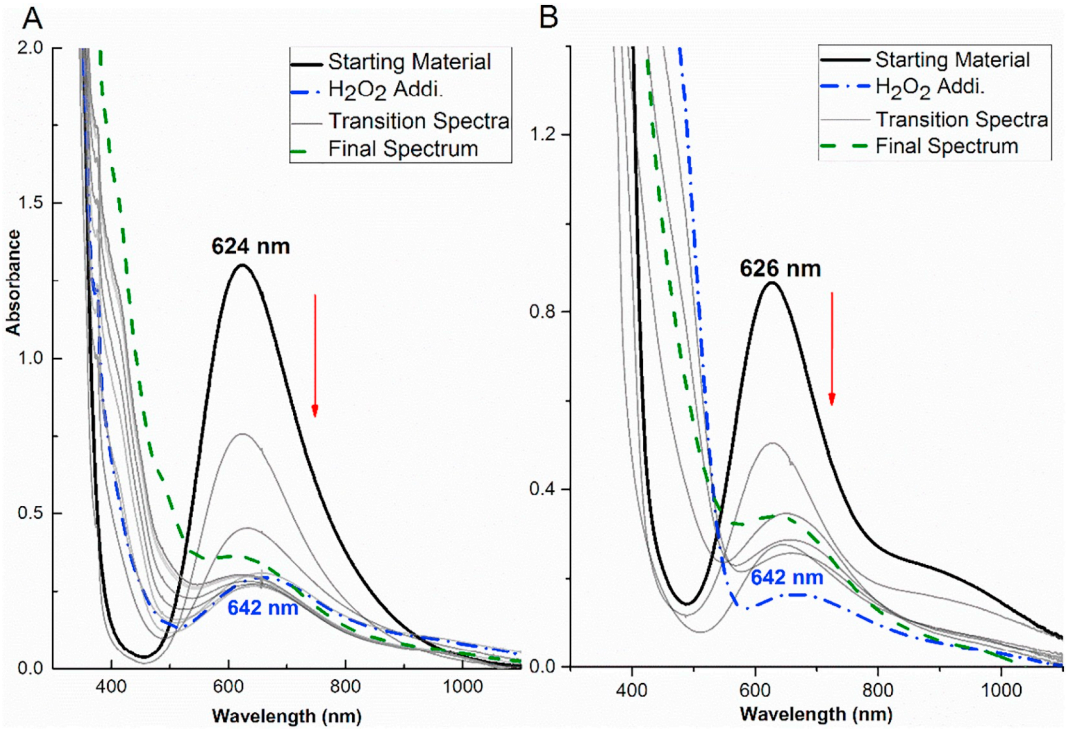

Fig. 10. Optical changes of complex **1** (panel A) and **2** (panel B) with H_2O_2/NEt_3 in the presence of excess DHA in acetonitrile at room temperature. Spectrum of starting material (in black solid line), final spectrum (in green dashed line). Grey lines represent spectral changes over time in a 1-cm path length cuvette.

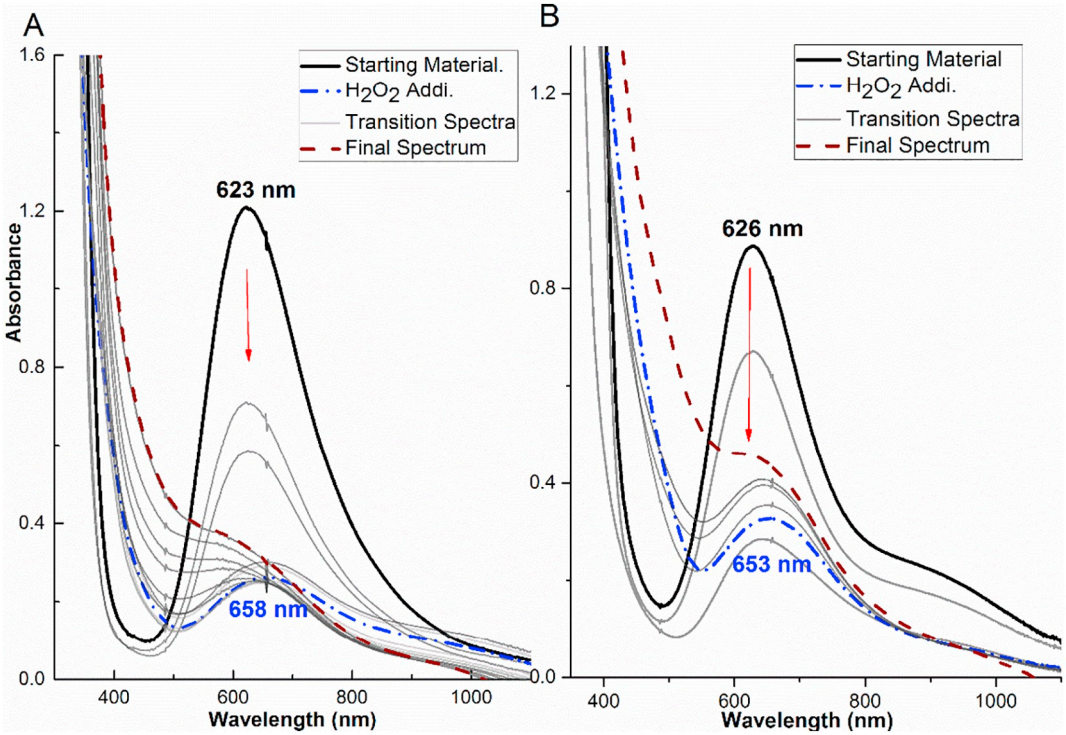

Fig. 11. UV–Vis absorption spectrum of complex **1** (A) and **2** (B) with H_2O_2/NEt_3 in presence of excess CHD in acetonitrile at room temperature; starting material (in black solid line), final spectra (in brown dashed line). Grey lines represent spectral changes over the time in a 1-cm path length cuvette.

CHD as an external substrate (TS-1c, Fig. 12) to be higher in energy ($\Delta G^{\ddagger}$ = 29.1 kcal/mol) compared to H-abstraction from the CH_3 groups on the amine nitrogens, but still lower than other possible sites of H-abstraction from the ligand (Fig. S5).

Next, we considered the reactivity of a possible reduced copper species, **[1-OOH]** (Fig. S7), which could form via hydroperoxide coordination to a Cu^{I} center upon homolytic cleavage of the Cu—O bond in **[1-OOH]** $^{+}$ ($\Delta E^{\ddagger}$ = 21.0 kcal/mol, Fig. S6), as was recently proposed [9]. The computed $\Delta G^{\ddagger}$ values indicate that if **[1-OOH]** forms in solution, $Cu^{II}O^{\cdot -}$ species could be generated with heterolytic cleavage of the O—O bond in the presence of Et_3NH^{+} as the Bronsted acid ($\Delta G^{\ddagger}$ = 14.8 kcal/mol) (Fig. S7). Subsequent H-abstraction from the CH_3 groups (TS-2a, Fig. 13) or the benzylic CH_2 groups (TS-2b, Fig. 13) of the ligand are equally feasible, with $\Delta G^{\ddagger}$ values of 13.2 and 13.7 kcal/mol, respectively (see Fig. S8 for alternative C-H activation pathways with **[1-O]** $^{+}$). Furthermore, including quantum tunneling effects via the Skodje-Truhlar approximation yields activation barriers in a narrow range of (~5 kcal/mol) indicating that H-abstraction from different sites is quite feasible (Fig. S8) [31]. Interestingly, the reaction of the $Cu^{II}O^{\cdot -}$ intermediate with CHD proceeds with an even lower $\Delta G^{\ddagger}$ of 6.6 kcal/mol, in contrast to the Cu^{II}-OOH case. This is in accord with the experimental observation that the external substrate CHD can successfully intercept ligand oxidation. This latter finding implies that $Cu^{II}O^{\cdot -}$, but not Cu^{II}-OOH, could be the reactive species in solution.

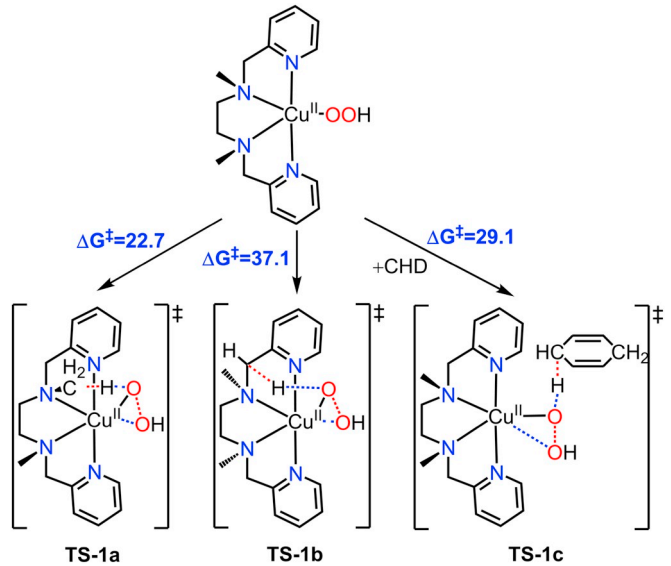

Fig. 12. C-H activation pathways via **[1-OOH]** $^{+}$ intermediate. Free energy changes are in units of kcal/mol.

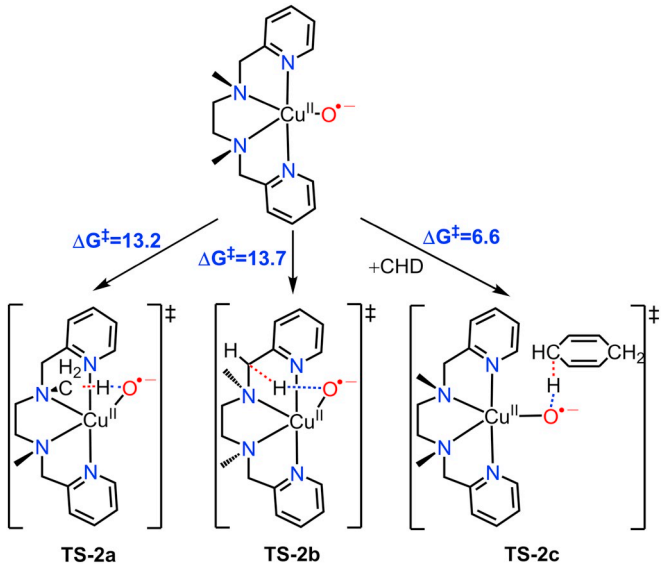

Fig. 13. C-H activation pathways via the **[1-O]** $^{+}$ intermediate. Free energy changes are in units of kcal/mol.

4. Conclusion

In summary, a new mononuclear Cu-system that reacts with H_2O_2/NEt_3 and performs both internal and external substrate oxidation is reported (Fig. 14). Our findings show that both **1** and **2** give higher yields of product with CHD substrate compared to DHA, likely as a consequence of the steric requirements of the latter. Spectroscopic characterization of **1** and **2** and their respective product solutions unequivocally establishes the mononuclear nature of both the starting material and the major product species. Computational calculations performed to understand the reaction mechanism suggest that a cupric-oxyl intermediate is the more likely reactive intermediate responsible for both ligand and external substrate oxidation.

These noteworthy results represent, to our knowledge, the first report of a copper system with H_2O_2 as the oxidant where all three modes of reactivity are observed: ligand oxidation, oxo-transfer to phosphine, and external hydrocarbon substrate oxidation. Clearly, the mechanistic underpinning of this system requires a thorough investigation at low temperature. Work in our laboratory is ongoing to trap and spectroscopically investigate the reactive intermediate in these transformations and establish its electronic structure.

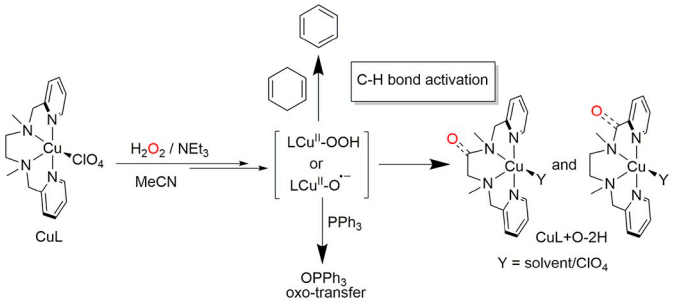

Fig. 14. Reactivity of **1** with H_2O_2 in MeCN in the presence and absence of substrate. (**2** exhibits similar reactivity).

Abbreviations

BPMEN	*N*,*N*′-dimethyl-*N*,*N*′-bis-(pyridine-2-ylmethyl)-1,2-diaminoethane
BQDMEN	*N*,*N*′-dimethyl-*N*,*N*′-bis-(quinoline-2-ylmethyl)-1,2-diaminoethane
DHA	9,10-dihydroanthracene
UV–Vis	Ultraviolet–Visible
ESI-MS	Electrospray ionization mass spectrometry
NMR	Nuclear magnetic resonance
HMBC	Heteronuclear multiple bond correlation
gc2hmbc	standard crisis2 heteronuclear multiple bond correlation
EPR	Electron paramagnetic resonance
MeCN	Acetonitrile
DCM	Dichloromethane
XAS	X-ray absorption spectroscopy
EXAFS	Extended X-ray absorption fine structure
DOSY	Diffusion-ordered spectroscopy
GC–MS	Gas chromatography–mass spectrometry
FID	Flame ionization detector
TDDFT	Time-dependent density functional theory
TS	Transition State
SCE	Saturated calomel electrode
XANES	X-ray absorption near edge structure
CHD	Cyclohexadiene

Acknowledgements

This work was supported by The University of Alabama in Huntsville. A. M. graciously thanks the University of Alabama in Huntsville for the NFR and IIDR award. Dr. Bernhard Vogler is graciously acknowledged for his insight and assistance with collecting data at the NMR facility of the University of Alabama in Huntsville. This material is based upon work supported by the U.S. Department of Energy, Office of Science, Office of Basic Energy Sciences, Division of Chemical Sciences, Geosciences, and Biosciences, under contract number DE-AC02-06CH11357 at Argonne National Laboratory (J.N. and O.G.P.). The work carried out at Brookhaven National Laboratory (M.Z.E.) was supported by the U.S. Department of Energy, Office of Science, Division of Chemical Sciences, Geosciences, & Biosciences, Office of Basic Energy Sciences under contract DE-SC0012704 and used resources of the Center for Functional Nanomaterials, which is a U.S. DOE Office of Science Facility, at Brookhaven National Laboratory under Contract No. DE-SC0012704. XAS measurements at SSRL were made possible by support from the National Institutes of Health (P30-EB-009998 and P41-GM-103393) and the Department of Energy, Office of Science, Office of Basic Energy Sciences (contract DE-AC02-76SF00515 to SSRL, SLAC National Accelerator Laboratory; contract DE-SC0012704 to NSLS-II, Brookhaven National Laboratory).

Notes

The authors declare no competing financial interest.

Appendix A. Supplementary data

Supplementary data to this article can be found online at https://doi.org/10.1016/j.jinorgbio.2019.03.014.

References

[1] L. Que Jr., W.B. Tolman, Biologically inspired oxidation catalysis, Nature (London, U. K.) 455 (7211) (2008) 333–340.
[2] J.P. Klinman, The copper-enzyme family of dopamine β-monooxygenase and peptidylglycine α-hydroxylating monooxygenase: resolving the chemical pathway for substrate hydroxylation, J. Biol. Chem. 281 (6) (2006) 3013–3016.
[3] D. Maiti, A.A. Narducci Sarjeant, K.D. Karlin, Copper(II)-hydroperoxo complex induced oxidative *N*-dealkylation chemistry, J. Am. Chem. Soc. 129 (21) (2007) 6720–6721.
[4] C.E. Elwell, N.L. Gagnon, B.D. Neisen, D. Dhar, A.D. Spaeth, G.M. Yee, W.B. Tolman, Copper-oxygen complexes revisited: structures, spectroscopy, and reactivity, Chem. Rev. 117 (3) (2017) 2059–2107.
[5] (a) Kodera, M.; Kita, T.; Miura, I.; Nakayama, N.; Kawata, T.; Kano, K.; Hirota, S., Hydroperoxo-copper(II) complex stabilized by N3S-type ligand having a phenyl Thioether. J. Am. Chem. Soc. 2001, 123 (31), 7715–7716; (b) Kim, S.; Lee, J. Y.; Cowley, R. E.; Ginsbach, J. W.; Siegler, M. A.; Solomon, E. I.; Karlin, K. D., A N3S (thioether)-ligated CuII-Superoxo with enhanced reactivity. J. Am. Chem. Soc. 2015, 137 (8), 2796–2799.
[6] T. Fujii, A. Naito, S. Yamaguchi, A. Wada, Y. Funahashi, K. Jitsukawa, S. Nagatomo, T. Kitagawa, H. Masuda, Construction of a square-planar hydroperoxo-copper(II) complex inducing a higher catalytic reactivity, Chem. Commun. (Cambridge, U. K.) 21 (2003) 2700–2701.
[7] Y.J. Choi, K.-B. Cho, M. Kubo, T. Ogura, K.D. Karlin, J. Cho, W. Nam, Spectroscopic and computational characterization of CuII-OOR (=R = H or cumyl) complexes bearing a Me6-tren ligand, Dalton Trans. 40 (10) (2011) 2234–2241.
[8] D. Maiti, H.R. Lucas, A.A. Narducci Sarjeant, K.D. Karlin, Aryl hydroxylation from a mononuclear copper-hydroperoxo species, J. Am. Chem. Soc. 129 (22) (2007) 6998–6999.
[9] S. Kim, J.W. Ginsbach, J.Y. Lee, R.L. Peterson, J.J. Liu, M.A. Siegler, A.A. Sarjeant, E.I. Solomon, K.D. Karlin, Amine oxidative *N*-dealkylation via cupric hydroperoxide Cu-OOH homolytic cleavage followed by site-specific Fenton chemistry, J. Am. Chem. Soc. 137 (8) (2015) 2867–2874.
[10] A.N. Campbell, S.S. Stahl, Overcoming the "oxidant problem": strategies to use O2 as the oxidant in organometallic C−H oxidation reactions catalyzed by Pd (and Cu), Acc. Chem. Res. 45 (6) (2012) 851–863.
[11] Singh, N.; Niklas, J.; Poluektov, O.; Van Heuvelen, K. M.; Mukherjee, A., Mononuclear nickel (II) and copper (II) coordination complexes supported by bispicen ligand derivatives: experimental and computational studies. Inorg. Chim. Acta 2017, 455 (Part_1), 221–230.
[12] Armarego, W. L. F.; Chai, C., Purification of Laboratory Chemicals, 5th Edition. Butterworth-Heinemann: 2003; (p 608).
[13] S. Stoll, A. Schweiger, EasySpin, a comprehensive software package for spectral simulation and analysis in EPR, J. Magn. Reson. 178 (1) (2006) 42–55.
[14] B. Ravel, M. Newville, ATHENA, ARTEMIS, HEPHAESTUS: data analysis for X-ray absorption spectroscopy using IFEFFIT, J. Synchrotron Radiat. 12 (4) (2005)

537–541.
[15] L. Chaloner, A. Khomutovskaya, F. Thomas, X. Ottenwaelder, Supramolecular control of monooxygenase reactivity in a copper(II) cryptate, Dalton Trans. 45 (27) (2016) 11109–11119.
[16] T.D.W. Claridge, I. Perez-Victoria, Enhanced ^{13}C resolution in semi-selective HMBC: a band-selective, constant-time HMBC for complex organic structure elucidation by NMR, Org. Biomol. Chem. 1 (21) (2003) 3632–3634.
[17] T.D.W. Claridge, High-Resolution NMR Techniques in Organic Chemistry, 3rd edition, Elsevier Science B.V, 2016 (p 552).
[18] Y. Zhao, D.G. Truhlar, A new local density functional for main-group thermochemistry, transition metal bonding, thermochemical kinetics, and noncovalent interactions, J. Chem. Phys. 125 (19) (2006) 194101.
[19] M. Dolg, U. Wedig, H. Stoll, H. Preuss, Energy-adjusted ab initio pseudopotentials for the first row transition elements, J. Chem. Phys. 86 (2) (1987) 866–872.
[20] W.J.R.,.L. Hehre, P.v.R. Schleyer, J.A. Pople, Ab Initio Molecular Orbital Theory, Wiley, New York, 1986.
[21] M.J. Frisch, G.W. Trucks, H.B. Schlegel, G.E. Scuseria, M.A. Robb, J.R. Cheeseman, G. Scalmani, V. Barone, B. Mennucci, G.A. Petersson, H. Nakatsuji, M. Caricato, X. Li, H.P. Hratchian, A.F. Izmaylov, J. Bloino, G. Zheng, J.L. Sonnenberg, M. Hada, M. Ehara, K. Toyota, R. Fukuda, J. Hasegawa, M. Ishida, N. Nakajima, Y. Honda, O. Kitao, H. Nakai, T. Vreven, A. Montgomery, J.E. Peralta, F. Ogliaro, M. Bearpark, J.J. Heyd, E. Brothers, K.N. Kudin, V.N. Staroverov, T. Keith, R. Kobayashi, J. Normand, K. Raghavachari, A. Rendell, J.C. Burant, S.S. Iyengar, J. Tomasi, M. Cossi, N. Rega, J.M. Millam, M. Klene, J.E. Knox, J.B. Cross, V. Bakken, C. Adamo, J. Jaramillo, R. Gomperts, R.E. Stratmann, O. Yazyev, A.J. Austin, R. Cammi, C. Pomelli, J.W. Ochterski, R.L. Martin, K. Morokuma, V.G. Zakrzewski, G.A. Voth, P. Salvador, J.J. Dannenberg, S. Dapprich, A.D. Daniels, O. Farkas, J.B. Foresman, J.V. Ortiz, J. Cioslowski, D.J. Fox, Gaussian 09, Revision D.01, Gaussian, I., Ed., Wallingford, CT, 2013.
[22] C.J. Cramer, Essentials of Computational Chemistry: Theories and Models, John Wiley & Sons Ltd, (2002), p. 562.
[23] A.V. Marenich, C.J. Cramer, D.G. Truhlar, Universal solvation model based on solute electron density and on a continuum model of the solvent defined by the bulk dielectric constant and atomic surface tensions, J. Phys. Chem. B 113 (18) (2009) 6378–6396.
[24] A.D. Becke, Density-functional thermochemistry. III. The role of exact exchange, J. Chem. Phys. 98 (7) (1993) 5648–5652.
[25] G. Scalmani, M.J. Frisch, B. Mennucci, J. Tomasi, R. Cammi, V. Barone, Geometries and properties of excited states in the gas phase and in solution: theory and application of a time-dependent density functional theory polarizable continuum model, J. Chem. Phys. 124 (9) (2006) 094107/1–094107/15.
[26] J.A. Keith, K.A. Grice, C.P. Kubiak, E.A. Carter, Elucidation of the selectivity of proton-dependent electrocatalytic CO_2 reduction by fac-Re(bpy)(CO)3Cl, J. Am. Chem. Soc. 135 (42) (2013) 15823–15829.
[27] (a) Maiti, D.; Narducci Sarjeant, A. A.; Karlin, K. D., Copper-hydroperoxo-mediated *N*-debenzylation chemistry mimicking aspects of copper monooxygenases. Inorg. Chem. 2008, 47 (19), 8736–8747; (b) Chaloner, L.; Askari, M. S.; Kutteh, A.; Schindler, S.; Ottenwaelder, X., Formation and reactivity of a biomimetic hydroperoxocopper(II) cryptate. Eur. J. Inorg. Chem. 2011, (27), 4204–4211; (c) Kunishita, A.; Teraoka, J.; Scanlon, J. D.; Matsumoto, T.; Suzuki, M.; Cramer, C. J.; Itoh, S., Aromatic hydroxylation reactivity of a mononuclear Cu(II)-alkylperoxo complex. J. Am. Chem. Soc. 2007, 129 (23), 7248–7249.
[28] (a) McLachlan, G. A.; Fallon, G. D.; Martin, R. L.; Spiccia, L., Synthesis, structure and properties of five-coordinate copper(II) complexes of pentadentate ligands with pyridyl pendant arms. Inorg. Chem. 1995, 34 (1), 254–61; (b) Tabbi, G.; Giuffrida, A.; Bonomo, R. P., Determination of formal redox potentials in aqueous solution of copper(II) complexes with ligands having nitrogen and oxygen donor atoms and comparison with their EPR and UV–vis spectral features. J. Inorg. Biochem. 2013, 128, 137–145; (c) Pilbrow, J. R., Transition Ion Electron Paramagnetic Resonance Oxford University Press: 1991, p 738; (d) Hathaway, B. J.; Billing, D. E., Electronic properties and stereochemistry of mononuclear complexes of the copper(II) ion. Coord. Chem. Rev. 1970, 5 (2), 143–207.
[29] I. Garcia-Bosch, M.A. Siegler, Copper-catalyzed oxidation of alkanes with H_2O_2 under a Fenton-like regime, Angew. Chem. Int. Ed. 55 (41) (2016) 12873–12876.
[30] Klein, J. E. M. N.; Dereli, B.; Que, L., Jr.; Cramer, C. J., Why metal-oxos react with dihydroanthracene and cyclohexadiene at comparable rates, despite having different C-H bond strengths. A computational study. Chem. Commun. (Cambridge, U. K.) 2016, 52 (69), 10509–10512.
[31] R.T. Skodje, D.G. Truhlar, Parabolic tunneling calculations, J. Phys. Chem. 85 (6) (1981) 624–628.